# THE SOLUBILITY OF AMORPHOUS ALUMINOUS SILICA: IMPLICATIONS FOR SCALING IN GEOTHERMAL POWER STATIONS

Julia K. Björke[1,2], Bruce W. Mountain[2] and Terry M. Seward[1]

[1]School of Geography, Environment and Earth Sciences, Victoria University of Wellington, Wellington, New Zealand

[2] GNS Science, 114, Karetoto Rd., Wairakei Research Centre, Taupo, New Zealand

j.bjorke@gns.cri.nz

**Keywords:** *Experimental geochemistry, amorphous aluminous silica scale, chemical zonation, solubility measurements*.

## ABSTRACT

Amorphous, aluminous silica (AAS) scale samples from the Wairakei and Ohaaki power stations, New Zealand, have been characterised chemically and mineralogically. These analyses show that Al is present in the amorphous phase and not in a distinct aluminosilicate mineral. SEM and EMPA analyses show chemical zonation of increased concentrations of Al, which correlates with the concentrations of Na, K and Ca.

The presence of Al makes the solubility of the scale dependent on pH and Al concentration and preliminary calculations show that amorphous aluminous silica can precipitate at temperatures as much as 25°C higher than of pure amorphous silica from geothermal brine.

One of the studied scales (SP3 2011) was used in a flow-through experiment at 100 - 200°C and pressures slightly above saturated water vapour pressure, using distilled water.

Preliminary solubility results show concentrations below pure amorphous silica saturation; however, it is not believed that saturation was reached in the experiments, at least at temperatures below 200°C. This conclusion is supported by the $Al/SiO_2$ ratio in the fluid.

## 1. INTRODUCTION

Scaling is a common problem in geothermal power plants; in particular it occurs from brines where minerals become saturated and precipitate. To prevent scaling, geochemists use thermodynamic modelling to apply appropriate treatment methods, such as adjusting temperature and/or pH. Generally, the thermodynamic properties of the minerals and the aqueous species involved in the chemical reactions are used. When adequate data are unavailable, an accurate assessment of scale formation becomes problematic.

Amorphous aluminous silica (AAS) scaling has been reported in many geothermal power plants such as in New Zealand, Indonesia, Philippines, Salton Sea, Japan and Iceland (Thórhallsson, 1975; Benevidez et al., 1988; Gunderson et al., 1995; Murray et al., 1995; Gallup, 1997; Yokoyama, 1993).

AAS scales typically deposit at higher temperatures than that of pure amorphous silica. In order to model their deposition and thus allow brine manipulation to prevent scaling, it is necessary to have accurate thermodynamic information on the properties of these scales. To date, the sole study on the solubility of amorphous aluminous silica was carried out by Gallup (1998). These were simple batch experiments in which there was no control on pH or Al concentration.

In the present study, we present results from the chemical and mineralogical analysis of a selection of AAS scales as well as solubility data for one AAS sample from an ongoing laboratory experiment at 100 - 200°C.

## 2. CHEMICAL AND MINERALOGICAL ANALYSIS

Four samples of AAS scale were collected at Wairakei (re-injection pipeline at Otupu) and Ohaaki (Separation Plant 3) geothermal power stations in the North Island of New Zealand (Fig.1). All samples precipitated from brine at a temperature of approximately 150°C and pH ≈ 8.

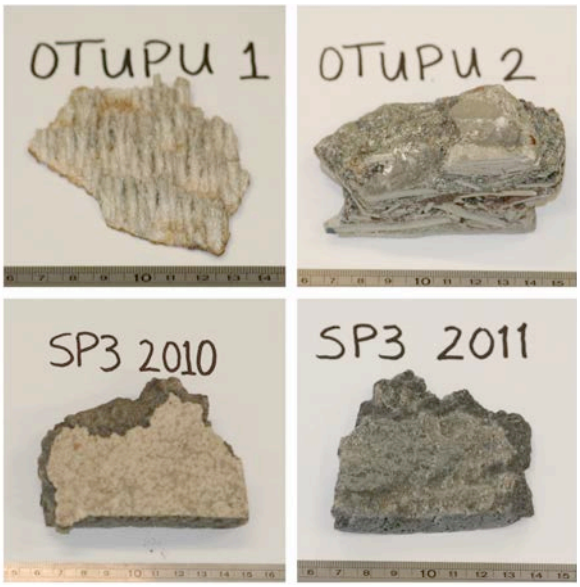


**Figure 1: The four samples of amorphous, aluminous silica scale (AAS). The top two figures are samples from Wairakei geothermal power station re-injection line. The two lower figures are from Ohaaki geothermal power station Separation Plant 3, sampled in 2010 and 2011. Scales are in centimeters.**

The AAS samples were analysed using X-ray diffractometry (XRD), X-ray fluorescence (XRF) Scanning Electron Microscopy (SEM) using Energy-Dispersive X-ray Spectroscopy (EDS) and Electron Probe Microanalysis (EMPA) in order to characterise the samples and verify that Al was not present in a Al-bearing mineral, distinct from the amorphous silica.

XRD analysis shows the sample is composed of mostly amorphous material with minor quartz, trace calcite, pyrite and biotite in all samples (Fig.2).

XRF results are shown in Table 1. Concentrations of $SiO_2$ ranged from 73.89-76.70%, $Al_2O_3$ from 8.38-10.46%, $K_2O$ from, 2.13-3.05%, $Na_2O$ from 1.71-2.15%, CaO from 1.08-2.13% and MgO from 0. 06-1.99%. Other oxides were less than 1% of the total sample.

**Table 1: Major oxide analysis of AAS scales. LOI is loss on ignition at 1000°C for 1 hour. Results are expressed as weight % on oven dried material at 110°C.**

| SAMPLE | Otupu 1 | Otupu 2 | SP3 2010 | SP3 2011 |
|---|---|---|---|---|
| $Fe_2O_3$ | 0.38 | 2.05 | 1.09 | 2.33 |
| MnO | 0.01 | 0.20 | 0.04 | 0.03 |
| $TiO_2$ | 0.02 | 0.10 | 0.04 | 0.08 |
| CaO | 1.91 | 2.13 | 1.50 | 1.08 |
| $K_2O$ | 2.79 | 2.13 | 3.05 | 2.85 |
| $P_2O_5$ | 0.01 | 0.04 | 0.02 | 0.03 |
| $SiO_2$ | 73.89 | 75.02 | 76.36 | 76.70 |
| $Al_2O_3$ | 10.46 | 8.71 | 8.54 | 8.38 |
| MgO | 0.06 | 1.99 | 0.67 | 0.14 |
| $Na_2O$ | 2.15 | 1.72 | 2.10 | 1.96 |
| LOI | 8.14 | 5.57 | 6.38 | 6.03 |
| SUM | 99.82 | 99.67 | 99.78 | 99.61 |

Figure 3 shows a plot of the $Al_2O_3$ versus total alkalis. There is a strong positive correlation between these parameters suggesting that the alkalis are incorporated into the AAS structure and are not solely present in other minor phases.

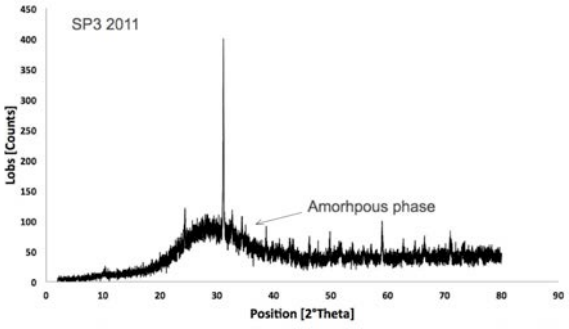


**Figure 2: X-Ray Diffractogram showing typical peaks for a AAS scale. The broad peak between 20 – 40 $2^o\theta$ is amorphous material; other peaks are quartz and minor calcite, pyrite and biotite.**

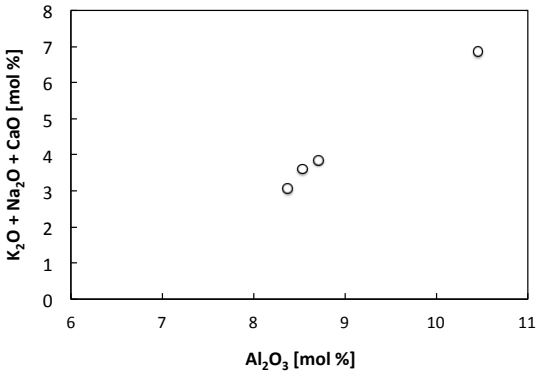


**Figure 3: Total alkali oxide concentrations versus $Al_2O_3$.**

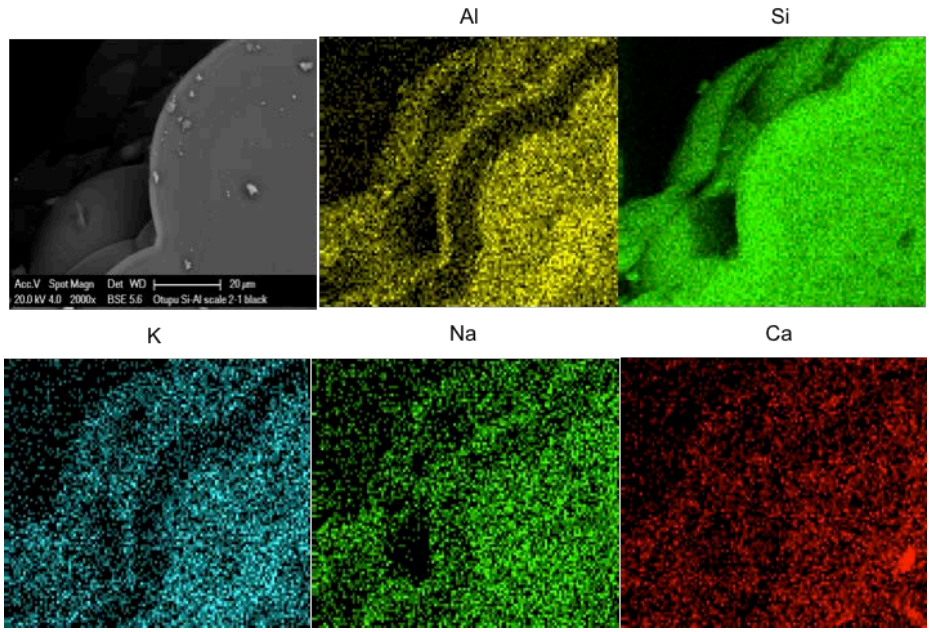


**Figure 4: EDS maps of a cross section through a silica spherule. Al, Na, K and to some extent Ca where present in the amorphous silica matrix and their concentrations increased with decreasing levels of silica. The spherulitic texture is evident in the SEM image in which chemical zonation is indicated by varying grey tones. Elemental maps show layering rich in Al which correlate spatially with areas of high K and Na concentration. This observation is somewhat less conclusive with Ca.**

SEM-EDS examination verified the results found by XRD and XRF analysis and revealed a spherulitic texture typical of silica spherules. EDS maps of a cross section through AAS sample Otupu 1 showed a chemical change within a silica spherule (Fig. 4). Al, Na, K and to some extent Ca were present in the amorphous silica matrix and their concentrations increased with decreasing levels of silica. The spherulitic texture is evident in the SEM image in which chemical zonation is indicated by varying grey tones. Elemental maps show layering rich in Al which correlate spatially with areas of high K and Na concentration. This observation is less conclusive with Ca.

In Figure 5, an EMPA traverse perpendicular to the layering in sample SP3 2010, shows variation in $Al_2O_3$ and the alkalis. At the outer surface (0.18 – 0.2 mm), there is a correlation between $Al_2O_3$ concentration and alkali content; however, the entire traverse shows high $Al_2O_3$ and alkalis.

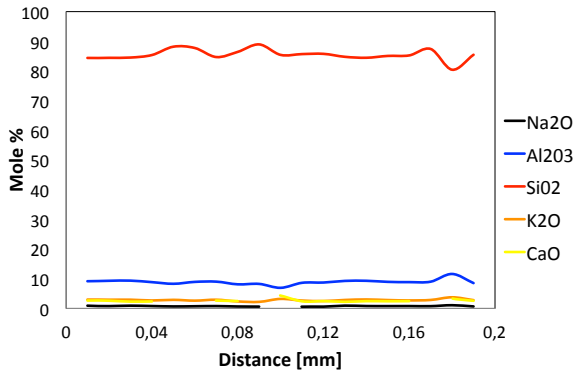


**Figure 5: Graph showing EMPA line analysis. There is an inverse correlation between $SiO_2$ and $Al_2O_3$ that is particularly evident between 0.18-0.20 mm.**

## 3. THERMODYNAMIC CALCULATIONS

Gallup (1998) measured the solubility of an AAS scale from Tiwi, Philippines in water between 25 – 250°C in the laboratory. He found that the solubility of AAS had a dependence on aluminium concentration and pH. Silica and aluminium concentrations were at their lowest at near-neutral pH while at pH<5 and >9, the kinetics of silica polymerisation and AAS deposition were inhibited. The conclusion from the experimental results was that the deposition of AAS is pH dependent and can occur between 25 and 75°C below the saturation point of pure amorphous silica.

Solubility data from Gallup (1998) have been used to calculate preliminary thermodynamic data for AAS. Note that these estimates ignore the Al concentration and pH dependence of AAS solubility and are thus only truly applicable to near-neutral brines. Figure 6 shows the saturation index of AAS and pure amorphous silica versus temperature for a flashed and cooled Ohaaki brine. AAS saturation occurs at a temperature approximately 25°C higher than pure amorphous silica.

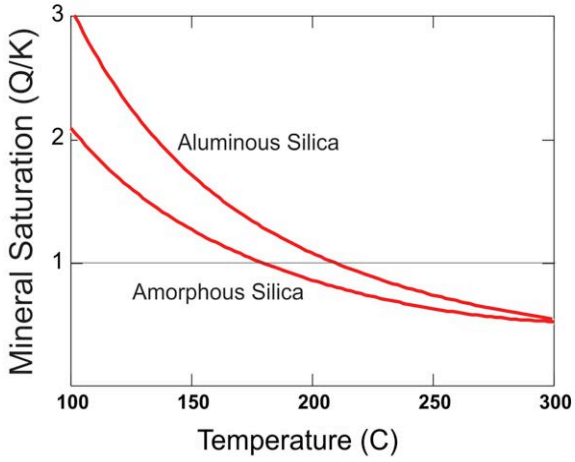


**Figure 6: Mineral saturation versus temperature for a flashed and cooled Ohaaki brine based on the solubility of amorphous silica of Gunnarsson and Arnórsson(2000) and AAS solubility of Gallup (1998).**

A general reaction that can be written for the solubility of AAS scale as Al hydroxide complexes:

$$xH_4SiO_4 + y[Al(OH)_n^{3-n}] + (n-3)y\ H^+ = xSiO_2.yAlO_{1.5} + (yn + 2x - 1.5y)\ H_2O$$

It can be seen the deposition/solubility of AAS is pH dependent and the slope of this dependence is (n-3). When n=0 ($Al^{3+}$). the log solubility dependence is -3 with pH. If n=3 ($Al(OH)_3^o$), the dependence is independent of pH whereas when n=4 ($Al(OH)_4^-$) the dependence is +1 with pH. This can be seen in Figure 7 in which the solubility of a hypothetical AAS phase is plotted as a function of pH. As noted by Gallup (1998), the solubility of AAS increases in the acid and alkali regions. Although the overall solubility of the AAS is dependent on the ratio x:y, the pH dependence of the solubility is not dependent on this ratio and hence the composition of the AAS.

## 4. EXPERIMENTAL DESIGN

The most homogeneous AAS scale was chosen for the solubility experiments (SP3 2011). The sample was crushed, sieved to 90-180 μm and washed with distilled water and ethanol before packing into a 0.635 x 20 cm stainless steel column. SEM examination showed that the AAS fragments surfaces had been sufficiently cleaned of fine material (Fig. 8).

Figure 9 shows the experimental set-up. A HPLC pump was used to pump distilled water through the column at 0.1 - 1 ml/hr. Temperature was controlled by placing the column in a oven. Pressure was controlled with at back pressure regulator and maintained at a few bar above saturated water vapor pressure to prevent boiling. The sample line out of the oven and the back pressure regulator were kept at a temperature slightly below 100°C, low enough to prevent boiling on the low pressure side but high enough to minimise silica precipitation in the back pressure regulator. Samples were analysed for cations by ICP-OES and for pH by potentiometry.

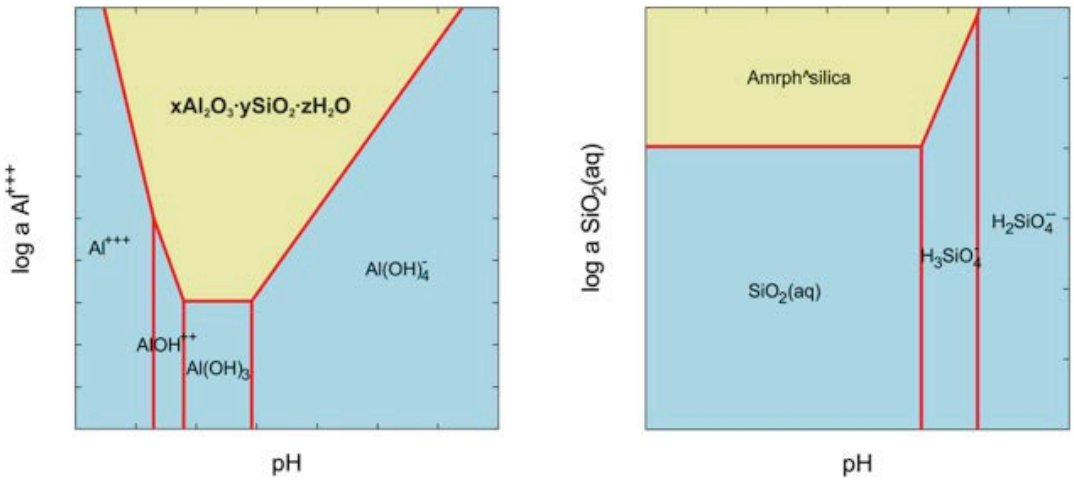


**Figure 7: Solubility of a hypothetical AAS phase as $Al(OH)_n^{3-n}$ (at fixed $a_{H4SiO4}$) and that of pure amorphous silica as $H_4SiO_4$. In the left diagram it can be seen that the hypothetical phase's solubility is dependent on pH while pure amorphous silica solubility is only pH dependent in the highly alkaline region.**

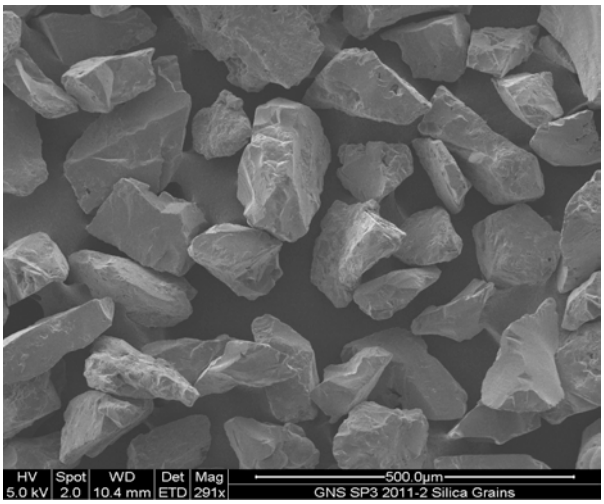


**Figure 8: SEM micrograph of the sample material used in the experiment.**

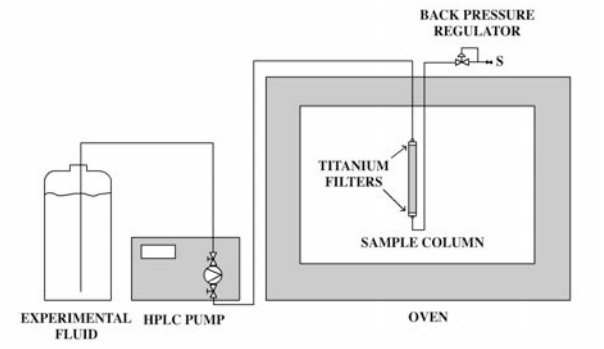


**Figure 9: Schematic illustration of the flow through apparatus.**

## 5. EXPERIMENTAL RESULTS

Results from the flow-through experiment can be seen in Figures 10 and 11. Sample numbers refer to the order in which the sample was taken during the course of the experiment (approximately 1 sample taken per day).

At 100°C, and a flow rate of 1.0 ml/hr, the $SiO_2$ concentration was 60 ppm. When flow rate was decreased to 0.5 ml/hr the concentration increased to approximately 80 ppm. The equilibrium solubility of pure amorphous silica at 100°C is 400 ppm (Gunnarsson and Arnórsson, 2000). Clearly, the measured solubility is much less than expected; however, the dissolution of the AAS may be too slow to reach equilibrium at 100°C. The Al concentration reached a concentration of about 2 ppm and pH ranged from 7.9 – 8.3 during the 100°C period. Because the solubility was so low, it was decided to increase the temperature to 150°C and decrease the flow rate to 0.2 ml/hr.

At 150°C, the $SiO_2$ concentration increased but was very unstable at ~300 ppm. We attribute this to boiling in the back pressure regulator and possibly loss of $SiO_2$. The temperature of the heating tape was reduced to prevent this. An increase in flow rate to 0.5 ml/hr resulted in an increase in the $SiO_2$ concentration to 415 ppm while Al stabilised at 5 ppm. The equilibrium solubility of pure amorphous silica at 150°C is 607 ppm. A decrease in flow rate to 0.1 ml/hr results in $SiO_2$ increasing to 500 ppm. If the solubility was far from equilibrium saturation one would expect a five-fold increase in concentration; however, the increase was only about 20%. This indicates that the fluid is close to equilibrium saturation and well below the pure amorphous silica saturation of 607 ppm. Al decreased to ~3 ppm. The explanation for this is unknown but could represent the precipitation of a aluminosilicate phase such as kaolinite. The pH range during the 150°C period was 8.1 – 8.4.

A temperature and flow rate increase to 200°C and 1.2 ml/hr resulted in a rise in $SiO_2$ concentration to 800 ppm and Al to 8 ppm. The pH range during this period was 8.1 - 8.5. Equilibrium solubility of pure amorphous silica at

200°C is 930 ppm. Unfortunately, when flow rate was decreased to 0.5 ml/hr, $SiO_2$ concentrations unexpectedly decreased. This is attributed to precipitation in the back regulator at these high silica concentrations. Note that Al also decreased after flow rate change.

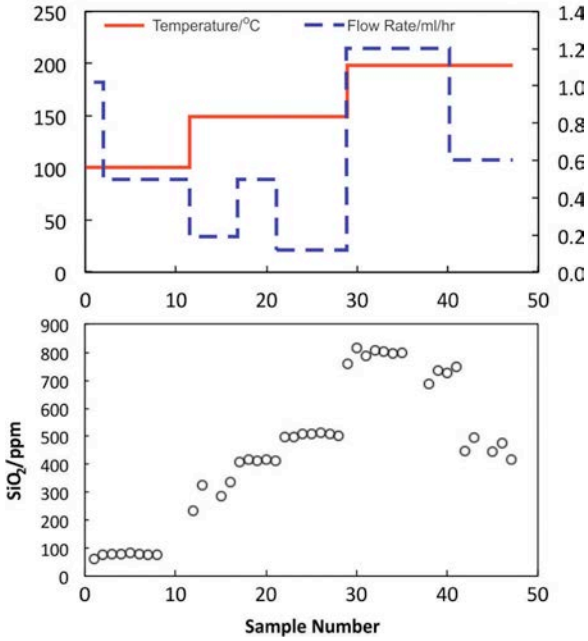


**Figure 10: Concentrations of $SiO_2$ in ppm. Sample number refers to the order of which the sample is taken. Approximately 1 sample was taken per day.**

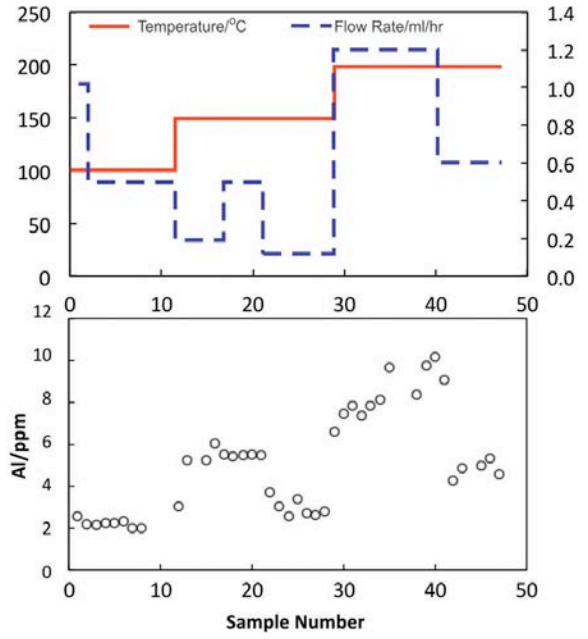


**Figure 11: Concentrations of Al in ppm. Sample number refers to the order of which the sample is taken. Approximately 1 sample was taken per day.**

Figure 12 shows the concentration of Al versus $SiO_2$ in the effluent. There is a broad correlation between these species ($r^2$=0.66). This positive correlation indicates that we have not reached an equilibrium with an aluminosilicate phase (at least at temperatures <200°C). If saturation has been reached at 200°C and 1.2 ml/hr then the solubility of AAS scale utilised is less than pure amorphous silica.

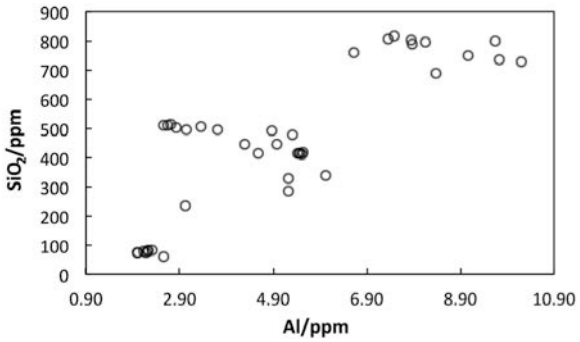


**Figure 12: Al versus $SiO_2$ concentration.**

## 6. CONCLUSIONS

Chemical and mineralogical analysis of four aluminous amorphous silica (AAS) scales have been performed. The results show that the scales are composed of mostly $SiO_2$ with significant concentration of $Al_2O_3$ and alkali metals. XRD analysis identifies mostly amorphous material with trace amounts of quartz, pyrite, calcite and biotite.

SEM-EDS analysis shows that the scales are zoned and there is a reasonable correlation between $Al_2O_3$ concentration and the alkali metals Na, K and Ca.

It is concluded that most of the $Al_2O_3$ in the scales comprises part of the amorphous phase.

A general reaction has been formulated to represent the solubility of AAS in $SiO_2$ - $Al(OH)_n^{n-3}$ – pH space. This reaction is used to show that the pH dependence of the solubility of an aluminosilicate phase (including AAS) does not depend on the phase dissolving, at constant $SiO_2$. This means that the pH dependence of the solubility of AAS is not dependent on its $SiO_2/Al_2O_3$ ratio; however the base solubility of the phase is dependent on this ratio.

Preliminary solubility results show significantly lower values below pure amorphous silica saturation; however, it is not believed that saturation was reached in the experiments, at least at temperatures below 200°C. This conclusion is supported by the $Al/SiO_2$ ratio in the fluid.


## ACKNOWLEDGEMENTS

The study is funded through the GNS Science NZG programme, Power Station Chemistry Project. We wish to thank Briony Jones and Marshall Muller for laboratory assistance.

**REFERENCES**


Benevidez, P.J., Mosby, M.D., Leong, J.K. and Navarro, V.C. : Development and performance of the Bulalo geothermal field. *Proc. 10th NZ Geothermal Workshop, Auckland*, pp. 55-60. (1988).

Gallup, D.L.: Aluminum silicate scale formation and inhibition: Scale characterization and laboratory experiments. *Geothermics*, Vol. 26, No.4, pp. 483-499. (1997).

Gallup, D.L.: Aluminum silicate scale formation and inhibition (2): Scale solubilities and laboratory and field inhibition tests. *Geothermics*, Vol. 27, No.4, pp. 485-501. (1998).

Gunderson, R.P., Dobson, P.F, Sharp, W.D., Pudjianto, R. and Hasibuan, A.: Geology and thermal features of the Sarulla contract area, North Sumatra, Indonesia. *Proc. World Geothermal Congress, Florence*, Vol. 2 pp. 687-692. (1995).

Gunnarsson, I. and Arnórsson, S.: Amorphous silica solubility and the thermodynamic properties of $H_4SiO_4^0$ in the range of 0° to 350°C at Psat. *Geochimica et Cosmochimica Acta*, Vol. 64, No. 13, pp. 2295–2307. (2000).

Murray, L.E., Rohrs, D.T., Rossknecht, T.G., Aryawijaya, R. and Pudyastuti, K.: Resource evaluation and development strategy, Awibengkok field. *Proc. World Geothermal Congress, Florence*, Vol. 3 pp. 1525-1530. (1995).

Thórhallsson, S., Ragnars, K., Arnórsson, S. and Kristmanssdóttir, H.: Rapid scaling of silica in two distinct heating systems. *Proc. 2nd United Nations Symposium on the Development and Use of Geothermal Resources, San Fransisco*, 2, pp. 1445-1449. (1975).

Yokoyama, T., Sato, Y., Maeda, Y., Tarutani, T. and Itoi, R.: Silicious deposits formed from geothermal water. I. The major constituents and the existing states of iron and aluminum. *Geochemistry*, Vol. 27, pp. 375-384. (1993).